NJC

ROYAL SOCIETY OF CHEMISTRY

PAPER

View Article Online
View Journal | View Issue



Cite this: *New J. Chem.*, 2020, **44**, 7954

# A "turn-on" fluorescent and colorimetric chemodosimeter for selective detection of $Au^{3+}$ ions in solution and in live cells *via* $Au^{3+}$-induced hydrolysis of a rhodamine-derived Schiff base†

Sanchita Mondal, *[a] Saikat Kumar Manna,[b] Sudipta Pathak,[b] Aritri Ghosh,[c] Pallab Datta,[c] Debasish Mandal[d] and Subrata Mukhopadhyay [a]

Received 14th March 2020, Accepted 20th April 2020

DOI: 10.1039/d0nj01273d

rsc.li/njc

A chromogenic and "off–on" fluorogenic chemodosimeter (**L**) based on a naphthalene–rhodamine B derivative was designed, synthesized and characterized for the selective and sensitive detection of $Au^{3+}$ ions in mixed acetonitrile aqueous medium in the presence of other competitive analytes. Probe **L** displayed a 696-fold "turn-on" fluorescence signal enhancement toward $Au^{3+}$ ions with the detection limit of $Au^{3+}$ of about 1.51 μM. In the presence of $Au^{3+}$ ions, probe **L** also exhibited a visible color change from colorless to pink that could be easily identified by the naked eye. This colorimetric and fluorometric changes were mainly due to the $Au^{3+}$ ion-triggered imine bond (C=N) hydrolysis sensing mechanism. Moreover, theoretical calculations were performed to explain the experimental results. In addition to these features, the "off–on" probe was successfully used to monitor intracellular $Au^{3+}$ ions in living MC3T3 cells through fluorescence imaging.



## Introduction

Exploration of the chemistry of gold has attracted tremendous attention from the scientific community owing to its chemical, analytical, biological, environmental and medicinal importance.[1] Gold, one of the most significant noble metals, is widely used in the area of synthetic chemistry, nanomaterials science, surface chemistry, theoretical investigations, gold plating, sensing materials and electrical contacts.[2,3] For instance, gold nanoparticles are extensively used in drug carriers, gene delivery systems, bioimaging substances, biosensors, water purification systems, medicines and additives in cosmetics, and soaps.[4,5] Besides, ionic gold species ($Au^{3+}$ ions), in contrast to its elemental form, are commonly used as efficient catalysts in selective oxidation reactions and several organic chemical transformations, in particular for activating the alkyne bond towards nucleophilic addition.[6] In addition to their catalytic properties, gold ions also have anti-inflammatory properties and are applied as pharmaceuticals for the treatment of various human diseases including tuberculosis, rheumatic arthritis, cancer, asthma, malaria, AIDS, brain lesions, and asthma.[7,8] Again, gold ions serve as inhibitors of macrophages and polymorphonuclear leucocytes.[9] In spite of their fascinating medicinal and chemical properties, gold ions especially, $Au^{3+}$ ions, impact human health and the environment in an adverse manner as $Au^{3+}$ ions can strongly bind to DNA, enzymes and other biomolecules, thereby causing severe damage to the kidneys, liver and the nervous system.[10,11] Thus, there is a critical need for the development of selective, sensitive, efficient and convenient analytical techniques to monitor $Au^{3+}$ ions in the environment and living systems. Until now, various conventional analytical methods have been reported for the detection of gold ions such as inductively coupled plasma atomic emission spectrometry (ICP-AES), electrochemical assay, inductively coupled plasma mass spectrometry (ICP-MS), flame atomic absorption spectrometry (FAAS), anodic stripping voltammetry and graphite furnace atomic absorption spectrometry (GFAAS); but these techniques often require sophisticated and costly instrumentation, time consuming and complicated sample preparation steps and skilled individuals, making them unsuitable for real-time and in-field analysis.[12,13] Hence, chromogenic and fluorogenic methods of the spectral field have recently emerged as a highly proficient, reliable and desirable approach for quick detection of gold ions due to their

[a] *Department of Chemistry, Jadavpur University, Kolkata 700032, India. E-mail: mondalsanchita2011@gmail.com*

[b] *Department of Chemistry, Haldia Government College, Debhog, Purba Medinipur, West Bengal 721657, India*

[c] *Centre for Healthcare Science, Indian Institute of Engineering Science and Technology, Shibpur, Howrah 711103, India*

[d] *School of Chemistry and Biochemistry, Thapar Institute of Engineering and Technology, Patiala 147004, Punjab, India*

† Electronic supplementary information (ESI) available. See DOI: 10.1039/d0nj01273d

 

high selectivity, sensitivity, cost-effectiveness, easy sample preparation, speediness, nondestructive nature, reproducibility and real-time monitoring ability for biological samples.[14] Therefore, some fluorescent probes for $Au^{3+}$ ions have been developed with a variety of fluorophores including naphthalimide,[15] boron-dipyrromethene (BODIPY),[16] coumarin,[17] rhodamine,[18] and fluorescein[19] during the last decades. These fluorescent probes detect $Au^{3+}$ ions through different sensing mechanisms such as activation of the alkyne bond,[20] hydrolysis reaction,[21] desulfurization reaction,[22] and coordination-based approaches.[23] However, only a scarce number of rhodamine-based fluorescent probes have been made available to date for the detection of $Au^{3+}$ ions *via* a $Au^{3+}$ promoted C═N bond (Schiff base) hydrolysis mechanism.[24] The rhodamine framework is commonly employed to construct ''off–on'' fluorescent probes because of its outstanding photophysical properties such as a great fluorescence quantum yield, large absorption coefficient, high photo stability and relatively long absorption and emission wavelengths. Additionally, the spirolactam ring of rhodamine-based probes is colorless and non-fluorescent, but its ring-opened spirolactam form gives rise to a strong fluorescence emission intensity and a pink color in the presence of specific metal cations, enabling ''naked eye'' detection of metal ions.[25] Keeping the above criteria in mind, herein, we present a rhodamine–naphthalene based colorimetric and ''turn-on'' fluorescent chemodosimeter **L**, which can selectively and sensitively detect $Au^{3+}$ ions through spirolactam ring opening followed by hydrolysis reaction. Probe **L** exhibits superb selectivity and sensitivity for $Au^{3+}$ ions over other competitive interference agents. Moreover, the comparison between the present probe (**L**) and a few previously reported probes for $Au^{3+}$ ion detection is shown in Table S1 (ESI†). Our probe (**L**) shows improved efficacy and superiority over other reported probes in terms of its easy synthetic scheme, good synthetic yield, selectivity, sensitivity, dual sensing techniques (fluorescence and naked eye detection) and good detection limit. Additionally, bioimaging experiments indicated that chemodosimeter **L** can be utilized as a fluorescent probe for monitoring $Au^{3+}$ ions in living cells.

## Results and discussion

Chemodosimeter **L** was synthesized in three steps, as shown in Scheme 1. Rhodamine B hydrazide (**1**) was prepared following a literature procedure.[26]

Compound **2** was synthesized through a Schiff base condensation reaction of rhodamine B hydrazide and 4-hydroxy-1-napthaldehyde in 89% yield. Finally, probe **L** was synthesized by the reaction between compound **2** and 1-fluoro-2,4-dinitrobenzene with 85% yield. The structure of **L** was fully characterized by $^1$H NMR, $^{13}$C NMR, FT-IR, and mass spectroscopy (Fig. S1–S5, ESI†). The spirolactam form of **L** was confirmed by the presence of a characteristic peak near 67.91 ppm in the $^{13}$C NMR spectrum of **L** (Fig. S4, ESI†).

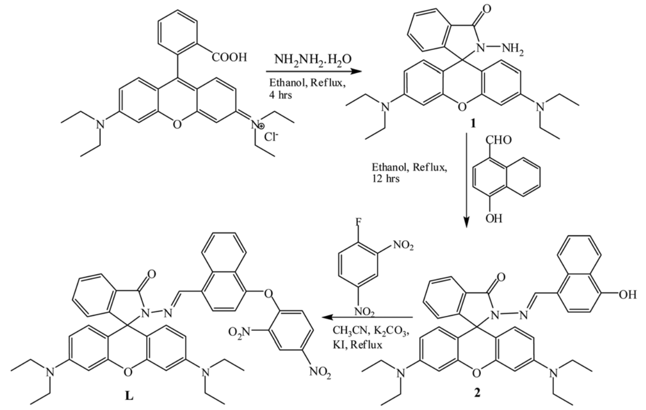


Scheme 1 The synthetic route of chemosensor **L**.

The UV-vis and fluorescence spectral responses of the probe **L** toward various metal cations ($Au^{3+}$, $Cr^{3+}$, $Mn^{2+}$, $Fe^{3+}$, $Co^{2+}$, $Ni^{2+}$, $Cu^{2+}$, $Zn^{2+}$, $Cd^{2+}$, $Pb^{2+}$, $Hg^{2+}$, $Pt^{2+}$, $Pd^{2+}$, $Al^{3+}$ and $Ag^+$), anions ($S^{2-}$, $HSO_4^-$, $HSO_3^-$, and $SO_3^{2-}$), amino acid (Cys) and reactive oxygen species ($ClO^-$, $H_2O_2$) were examined in $CH_3CN/H_2O$ (1 : 1, v/v, 10 mM HEPES buffer, and pH 7.4) solution. As shown in Fig. 1, the UV-vis spectrum of probe **L** displayed no noticeable absorption band above 500 nm, signifying the presence of the spirolactam form of **L**. Upon gradual addition of $Au^{3+}$ to a solution containing chemodosimeter **L**, a remarkable increase in absorbance at 560 nm was observed, which indicated that the ring-open delocalized spirocyclic structure of **L** became the major species in the inspected solution. In the presence of $Au^{3+}$ ions, the organo aqueous solution $CH_3CN/H_2O$ (1 : 1, v/v, 10 mM HEPES buffer, and pH 7.4) of **L** turned from colorless to pink (Fig. 1, inset), thus enabling the 'naked eye' detection of $Au^{3+}$ in environmental samples. Under similar conditions, no apparent absorption or color changes were observed in the presence of other interfering species (Fig. 1b and Fig. S7, ESI†), showing the high selectivity of **L** toward $Au^{3+}$.

The fluorometric titration of the $Au^{3+}$ ion was also performed under similar working conditions. The chemodosimeter **L** exhibited almost no obvious emission signal upon excitation at 560 nm (quantum yield $\phi$ = 0.001, ESI†). However, upon addition of $Au^{3+}$ ions to the solution of probe **L**, an amazing enhancement of fluorescence spectra at 588 nm was observed (quantum yield $\phi$ = 0.689, ESI†), accompanied by an emission color change from colorless to orange (Fig. 2a). The fluorescence intensity reached its maximum after addition of 1.5 equivalents of $Au^{3+}$ ions and it increased up to 696-fold, which was higher than the result obtained from the previously reported $Au^{3+}$ sensors.[27] Moreover, as shown in Fig. 2b, the observed emission intensity in the presence of $Au^{3+}$ ions gradually enhanced in a $Au^{3+}$ concentration-dependent manner. The above results suggested that the spirocyclic ring of probe **L** was opened and a conjugated structure was formed in the solution. In particular, the detection limit is an important factor for chemosensing applications. Now, the detection limit of **L** for $Au^{3+}$ was estimated to be 1.51 μM using fluorescence titration spectra

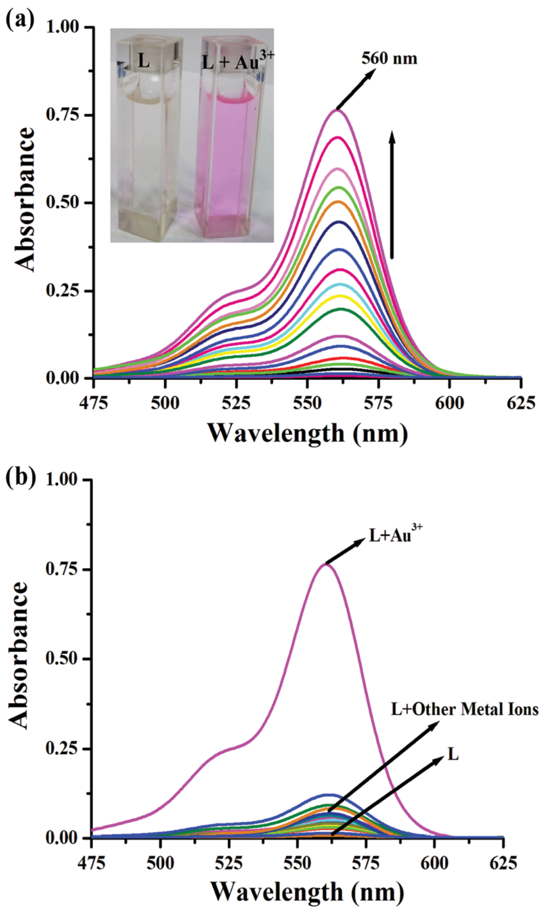


Fig. 1 (a) UV-vis absorption spectra of **L** ($1.0 \times 10^{-5}$ M) in the presence $Au^{3+}$ ions ($1.0 \times 10^{-4}$ M) in $CH_3CN/H_2O$ (1 : 1, v/v, 10 mM HEPES buffer, and pH 7.4) solution. Inset: Photographs of color changes of probe **L** upon addition of $Au^{3+}$ ions under visible light. (b) UV-vis absorption spectra of **L** in the presence of various metal ions in $CH_3CN/H_2O$ (1 : 1, v/v, 10 mM HEPES buffer, and pH 7.4) solution.

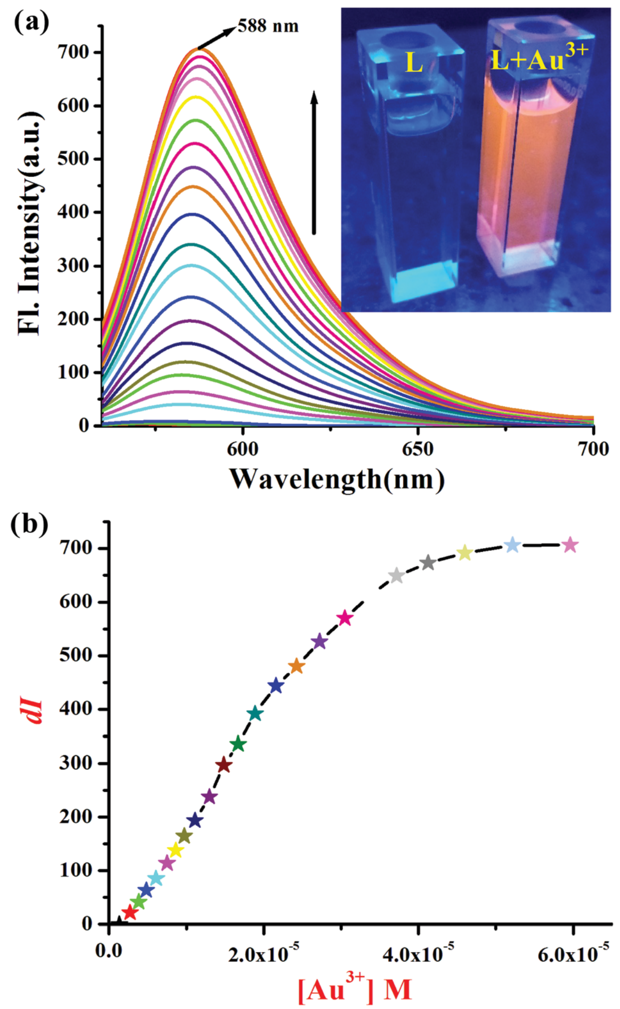


Fig. 2 (a) Fluorescence intensity changes of **L** ($1.0 \times 10^{-5}$ M) upon addition of $Au^{3+}$ ions ($1.0 \times 10^{-4}$ M) in $CH_3CN/H_2O$ (1 : 1, v/v, 10 mM HEPES buffer, and pH 7.4) solution. $\lambda_{ext}$ = 560 nm. Inset: Fluorescence photographic images of **L** and **L**$^{+}$ $Au^{3+}$. (b) Change of emission intensity at 588 nm with incremental addition of $Au^{3+}$ ($\lambda_{ext}$ = 560 nm).

based on the technique employed in earlier literature (Fig. S8, ESI†).[28] Moreover, time dependent fluorescence studies revealed that the chemodosimetric reaction of probe **L** with $Au^{3+}$ ions was very fast. As illustrated in Fig. S9 (ESI†), upon addition of $Au^{3+}$ ions to the probe solution, a remarkable increase in fluorescence signal was found within seconds and the complete enhancement of emission intensity at 588 nm was observed in 1.5 minutes, demonstrating that chemodosimeter **L** could be employed for real-time monitoring of $Au^{3+}$ in biological specimens.

To study the selectivity of probe **L** in practice, the fluorescence response of **L** toward various competitive analytes was examined in $CH_3CN/H_2O$ (1 : 1, v/v, 10 mM HEPES buffer, and pH 7.4) solution. As represented in Fig. 3 and Fig. S10 (ESI†), no obvious fluorescence enhancement or color change was observed upon addition of 10 equiv. of different metal ions, anions, amino acids and reactive oxygen species, whereas the emission intensity increased meaningfully after treatment with $Au^{3+}$ ions. Moreover, competition experiments were performed in the presence of 1.5 equiv. of $Au^{3+}$ ions mixed with 10 equivalents of other metal cations stated above, respectively.

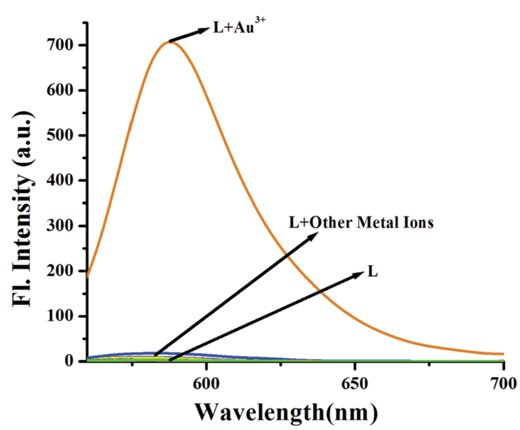


Fig. 3 Fluorescence emission spectra of **L** ($1.0 \times 10^{-5}$ M) in the presence of various metal ions in $CH_3CN/H_2O$ (1 : 1, v/v, 10 mM HEPES buffer, and pH 7.4) solution. $\lambda_{ext}$ = 560 nm.

The increase in the fluorescence intensity arising from the mixing of $Au^{3+}$ and other metal ions was analogous to that caused only by $Au^{3+}$ ions, suggesting that the $Au^{3+}$-induced fluorescence enhancement was not affected by other interfering metal ions (Fig. S11, ESI†). Hence, the above outcomes confirm the high selectivity of **L** for $Au^{3+}$ ions.

To get insight into the sensing mechanism of chemodosimeter **L** with $Au^{3+}$, we first examined whether the sensing process is reversible or irreversible. In order to verify this, an excess amount of the $Au^{3+}$ chelator tetra butyl ammonium cyanide (20 equiv.) ($^t$Bu$_4$NCN) was added to a solution of **L** pretreated with $Au^{3+}$ ions. As shown in Fig. S12 (ESI†), the absorption and fluorescence spectra induced by $Au^{3+}$ did not vary after addition of $^t$Bu$_4$NCN, suggesting the irreversible chemical reaction of this sensing process. Now, the result of the suggested reaction-based sensing process could be simply analyzed by using a thin layer chromatography (TLC) plate. After the reaction of **L** with $Au^{3+}$, a pink color and orange fluorescent spots appeared on the TLC plate, indicating the formation of the new rhodamine derivative (Fig. S13, ESI†). To confirm the sensing mechanism, ESI-MS analysis was carried out. As shown in Fig. S5 (ESI†), probe **L** without $Au^{3+}$ ions displayed a peak only at $m/z$ = 777.3034 (calcd = 776.2958), which corresponded to [**L** + H] $^+$. However, when 2 equiv. of $Au^{3+}$ ion was added into the solution of **L**, the peak of **L** ($m/z$ = 777.3034) totally disappeared and two new peaks appeared at $m/z$ 457.2900 and 443.2640, assigned to rhodamine hydrazide (**I$_2$**) and rhodamine B (**P**), respectively (Fig. S6, ESI†). These results supported our assumption that the overall sensing mechanism was associated with the $Au^{3+}$-promoted ring opening hydrolysis process. To further validate this hydrolysis reaction, the FT-IR study of **L** was performed before and after the addition of $Au^{3+}$ ions. Fig. S14 (ESI†) displays the FT IR spectra of **L** and there is no stretching band in the region of 3000–3500 cm$^{-1}$. Moreover, the FT-IR spectrum of **L** upon reaction with $Au^{3+}$ exhibited a strong frequency band at 3370 cm$^{-1}$ attributable to the –OH group of the newly formed rhodamine B, which was comparable with the FTIR spectrum of pure rhodamine B.[29] Therefore, the spectral studies confirmed that the interaction of $Au^{3+}$ ions with probe **L** occurred through a reaction-based chemodosimetic approach.

Taking the above observations together, a reasonable reaction mechanism is proposed in Scheme 2. Initially, $Au^{3+}$ ions rapidly coordinated to one oxygen and two nitrogen atoms in probe **L** and promoted the spirocyclic ring opening of **L** to form intermediate **I$_1$**. Then, fast hydrolysis of the C═N bond of the intermediate (**I$_1$**) by the attack of water first formed rhodamine hydrazide (**I$_2$**), which further hydrolyzed to rhodamine B (**P**), thus generating the emission color of the solution.

A complementary computational investigation[30,31] has been performed to further verify the experimental outcomes and the possible reasons behind the red-shifted absorptions of probe **L** in the presence of $Au^{3+}$. As proposed in the mechanistic section, probe **L** decomposed in the presence of $Au^{3+}$ and formed rhodamine hydrazide (**I$_2$**) and then rhodamine B (**P**) after hydrolysis (Scheme 2 and Fig. 4). So, we carried out a rigorous

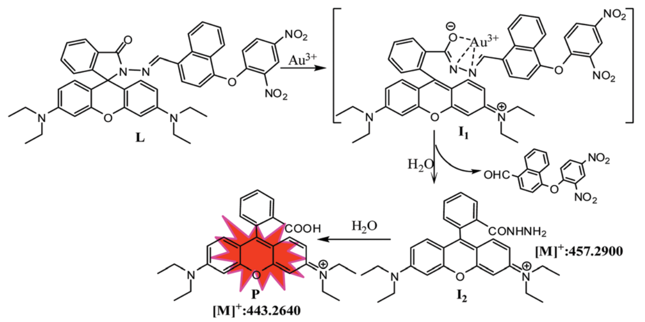


Scheme 2 Proposed $Au^{3+}$-promoted C═N bond hydrolysis reaction mechanism of probe **L**.

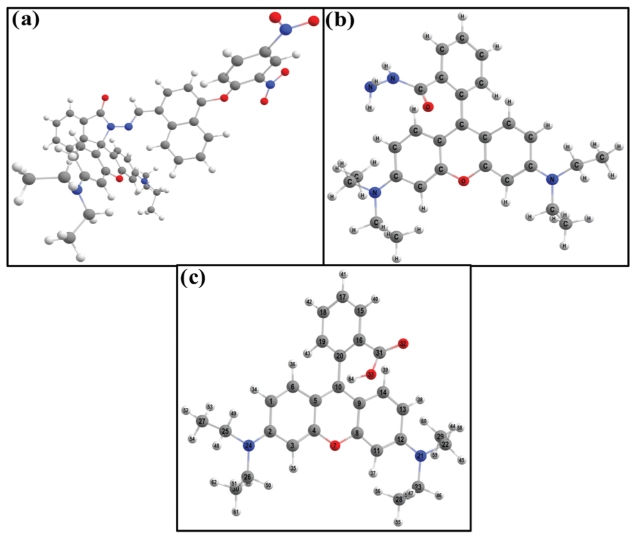


Fig. 4 The energy optimized structures of (a) **L**, (b) rhodamine hydrazide (**I$_2$**) and (c) rhodamine B (**P**).

time-dependent density functional theory investigation of **L**, **I$_2$** and **P**. The results indicate the presence of the main peaks in the case of **L**, **I$_2$** and **P** at 375 nm, 481 nm and at 491 nm (Table S2, ESI†), respectively.

The experimental observed absorption maxima of **L** and after addition of $Au^{3+}$ were found at 315 nm and 560 nm, respectively (Fig. S15, ESI†). From the aforementioned values, it is quite clear that the theoretical results are in good agreement with the experimental observation, which is able to justify completely the insights into the proposed $Au^{3+}$ sensor mechanism of **L**. The computed energies of the HOMO and the LUMO and their differences are also presented in Fig. S16 (ESI†). Apparently, the HOMO–LUMO gap looks unusual as it is higher for **I$_2$** and **P** than **L**, though a clear red shift can be observed (Table S3, ESI†). The anomaly can be explained by careful observation of the transition orbitals responsible for the absorption. In the case of **I$_2$** and **P**, the major contributing transitions are HOMO to LUMO, whereas for **L**, these transitions have no role in the absorption.

Due to the fluorescence 'turn-on' behavior of probe **L** for $Au^{3+}$ ions, probe **L** was then effectively employed in fluorescence

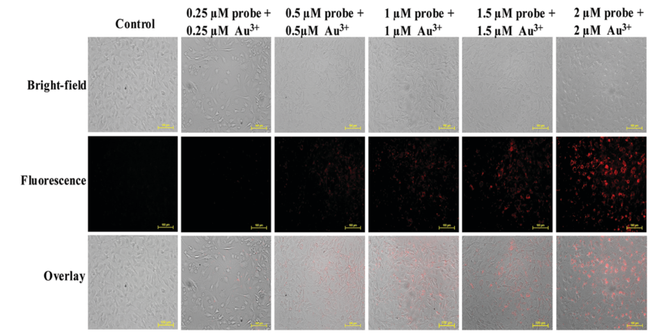


Fig. 5 Bright-field, fluorescence and overlay images of MC3T3 cells treated with **L** and $Au^{3+}$ ions.

microscopy investigation of $Au^{3+}$ ions in living cells. First, MC3T3 cells were treated with different concentrations of probe **L** (0.25, 0.5, 1, 1.5, and 2 μM) for 30 min at 37 °C and then washed with PBS buffer (pH 7.4) to eliminate the extra probes. Afterward, the treated cells were supplemented with 0.25, 0.5, 1, 1.5, and 2 μM $AuCl_3$ solutions and then incubated in the culture medium for 30 min at 37 °C. After washing with the PBS buffer, the incubated cells were successively imaged using a fluorescence microscope. As shown in Fig. 5, the MC3T3 cells loaded with both probe **L** and $Au^{3+}$ ions showed a substantial red fluorescence from the intracellular area, while the cells treated with either probe **L** or $Au^{3+}$ ions did not exhibit any perceptible fluorescence. However, the fluorescence intensity of the cells increased with increasing concentration of $Au^{3+}$ ions. In addition, there were no noteworthy gross morphological changes observed in the bright-field images of the cells, signifying that the cells were viable throughout the cell imaging experiments. The overlay of fluorescence and bright-field images established that the emission signals were located in the perinuclear region of the cytosol, showing a subcellular distribution of $Au^{3+}$ ions. The above results confirmed that probe **L** was cell permeable and could be employed for monitoring intracellular $Au^{3+}$ ions in living cells. Moreover, an MTT assay showed that probe **L** had low cytotoxicity to the living MC3T3 cells (Fig. S17, ESI†).

# Conclusions

In summary, we have devised naphthalene–rhodamine B derivative **L** as a colorimetric and ''turn-on'' chemodosimeter for $Au^{3+}$ ions based on $Au^{3+}$-promoted C═N bond (Schiff base) hydrolysis of probe **L** in organo-aqueous solution. Probe **L** has high sensitivity and selectivity toward $Au^{3+}$ ions in $CH_3CN/H_2O$ (1 : 1, v/v, 10 mM HEPES buffer, and pH 7.4) medium with significantly increased absorption and emission spectral intensity (696-fold), accompanied by a color change from colorless to strong orange fluorescence. From the fluorescence titration spectra, the detection limit of chemodosimeter **L** for $Au^{3+}$ ions was found to be 1.51 μM. More prominently, the fluorescence response of the probe in the presence of $Au^{3+}$ ions is also highly selective, as the hydrolysis reaction cannot be facilitated or interfered by a number of biologically important competitive analytes, achieving the selectivity necessary for any practical application. In addition, the theoretical calculations authenticate our experimental outcomes. Moreover, cell imaging studies have shown that the cell membrane permeable chemodosimeter **L** can be excellently used to detect intracellular $Au^{3+}$ ions in living MC3T3 cells. We believe that this chemodosimeter will be of potential interest to researchers for studying the various functions of $Au^{3+}$ ions in biological systems.

# Experimental section

## Materials and instruments

All the reagents for synthesis, solvents (analytical and spectroscopic grades) and cationic salts (chloride salts of $Au^{3+}$, $Cr^{3+}$, $Fe^{3+}$, $Zn^{2+}$, $Cd^{2+}$, $Pb^{2+}$, $Hg^{2+}$, $Pt^{2+}$, and $Pd^{2+}$, perchlorates of $Mn^{2+}$, $Co^{2+}$, $Ni^{2+}$, and $Cu^{2+}$, and nitrate salts of $Ag^{+}$ and $Al^{3+}$), anionic salts (sodium salts of $S^{2-}$, $HSO_4^{-}$, $HSO_3^{-}$, and $SO_3^{2-}$), amino acid (cysteine) and reactive oxygen species (NaOCl, and $H_2O_2$) were purchased from commercial suppliers and used without any extra purification. All solvents were dried according to standard processes. All reactions were examined by thin layer chromatography (TLC) plates with detection using a UV cabinet, and column chromatography was carried out using 60–120 mesh silica gel. Elix Millipore water was employed throughout all the analytical experiments. The $^{1}H$ NMR spectra and $^{13}C$ NMR were obtained using a Bruker 400 MHz spectrometer (at 400 MHz for $^{1}H$ and 100 MHz for $^{13}C$) with chemical shifts reported as ppm ($\delta$) units (in $CDCl_3$ solvent, TMS as an internal standard). Mass spectra were obtained using a HRMS QTOF Micro YA263 mass spectrometer. UV-visible and fluorescence spectra were obtained using a SHIMADZU UV-1800 spectrophotometer and a PerkinElmer LS-55 spectrofluorimeter, respectively. FT-IR spectra were obtained using a PerkinElmer FTIR spectrometer. The following abbreviations are utilized in the $^{1}H$ NMR spectrum to define spin multiplicities: s = singlet; d = doublet; t = triplet; and m = multiplet.

## Detection limit calculation

The detection limit of **L** for $Au^{3+}$ was calculated using the following equation:[28]

$$\text{Detection limit} = 3\text{Sb1}/S$$

where Sb1 is the standard deviation of the blank solution and $S$ is the slope of the calibration curve.

## General method for UV-vis and fluorescence titration experiments

All titrations were performed in $CH_3CN/H_2O$ ($CH_3CN/H_2O$ = 1 : 1, v/v, 10 mM HEPES buffer, and pH = 7.4) solution. Stock solutions of the probe **L** ($1 \times 10^{-5}$ M) were prepared in organo aqueous solution. Again, stock solutions of the analytes ($1 \times 10^{-4}$ M) were prepared in Millipore water. During titration, probe **L** solutions were positioned every time in a quartz optical cell (1.00 cm optical path length) and then analyte solutions were gradually added to it by using a micropipette.

### Computational details

The geometries were fully optimized by employing density functional theory (DFT) using Becke's three-parameter hybrid exchange functional and the Lee–Yang–Parr correlation functional (B3LYP) with the Pople's spilt-valence 6-31+G(d,p) basis set.[30] The frequency calculations have also been carried out to verify the exact minimum of the complex. TDDFT calculation has been performed at the same level of theory. All the calculations have been conducted using the Gaussian 16 program.[31]

### Cell imaging experiments

**Cell culture protocol.** MC3T3, a mouse precursor osteoblast cell line derived from *Mus musculus (mouse)* calvaria, was used in this study. The cells were maintained in a T25 polystyrene flask (Corning, USA) in complete α-MEM media (Gibco, Invitrogen Life Science Technologies, USA) with 10% FBS (Gibco, Invitrogen Life Science Technologies, USA) and 1% anti-biotic & anti-mycotic solution (Gibco, Invitrogen Life Science Technologies, USA) at 37 °C and 5% $CO_2$ in a humidified incubator (Esco-AC2-4S8). When the flask reached 70–80% confluency, cells were trypsinized with 0.05% trypsin–EDTA (Gibco, Invitrogen Life Science Technologies, USA) and used for *in vitro* studies.

**Cell viability assay.** For assessing the viability of the cells upon treatment with probe **L** solubilized in DMSO and $AuCl_3$, MTT assay was executed. In a 96-well plate, MC3T3 cells at a seeding density of $\sim 10^4$ cells per well were seeded and cultured overnight at 37 °C and 5% $CO_2$ in a humidified incubator (Esco-AC2-4S8). Different concentrations of probe **L** and $AuCl_3$ were used for the study (0.25, 0.5, 1, 1.5, and 2 μM). The cells were incubated with probe **L** first for 30 min in incomplete medium, washed with 1× PBS and then again re-incubated with $AuCl_3$ solution in incomplete medium for 30 min at 37 °C and 5% $CO_2$. After the incubation, 10% (v/v) MTT reagent (MTT assay kit-Himedia-CCK003) was added with fresh incomplete medium and further incubated for 4 h. Following this, the medium with MTT reagent was discarded and solubilization buffer provided with the kit was used to solubilize the formazan crystals formed within cell, and absorbance was read at 570 nm using a microplate reader (Thermo Scientific, USA). A reference measurement was also taken at the wavelength of 670 nm from all the wells. Cells without any treatment were kept as a control. The percentage cell viability was calculated as per the following equation.

$$\text{Cell viability }(\%) = \frac{[(\text{Abs570T} - \text{Abs670T}) - (\text{Abs570C} - \text{Abs670C})]}{(\text{Abs570C} - \text{Abs670C})} \times 100.$$

where T = treatment and C = control.

### Imaging studies

For imaging studies, $5 \times 10^4$ cells were seeded on 18 mm sterile glass coverslips and cultured overnight at 37 °C and in 5% $CO_2$ in a humidified incubator (Esco-AC2-4S8). The cells were treated with different concentrations of probe **L** and $AuCl_3$ (0.25, 0.5, 1, 1.5, and 2 μM) using the same protocol as for cell viability assay. The cells were washed with 1× PBS after treatment and images in DIC and fluorescence mode were acquired using a Nikon inverted fluorescence microscope (Nikon eclipse Ti, Japan) under 20× objectives (DIC and S-Plan Fluo).

### Synthesis

**Preparation of compound 2.** Rhodamine B hydrazide (**1**, 0.40 g, 0.88 mmol) was dissolved in 7 ml of ethanol with continuous stirring and then 0.15 g of 4-hydroxy-1-naphthaldehyde (0.88 mmol) in 5 ml of ethanol was added to the solution and heated to reflux for 12 h. The formed precipitate was filtered, washed with ethanol, and the residue left was crystallized from ethanol to give the yellow colored solid compound **2** in 89% yield. $^1$H NMR (DMSO-$d_6$, 400 MHz) $\delta$ (ppm): 1.06 (t, 12H, $J$ = 6.88 Hz, $-NCH_2CH_3$), 3.29 (t, 8H, $J$ = 11.36 Hz, $-NCH_2CH_3$), 6.35 (dd, 2H, $J$ = 7.84 Hz & 5.76 Hz), 6.45 (d, 4H, $J$ = 9.68 Hz), 6.86 (d, 1H, $J$ = 8 Hz), 7.15 (d, 1H, $J$ = 7.08 Hz), 7.38 (t, 1H, $J$ = 7.84 Hz), 7.45 (t, 1H, $J$ = 6.92 Hz), 7.50 (d, 1H, $J$ = 8.08 Hz), 7.56–7.64 (m, 2H), 7.91 (d, 1H, $J$ = 6.96 Hz), 8.14 (d, 1H, $J$ = 8.44 Hz), 8.24 (d, 1H, $J$ = 8.48 Hz), 9.27 (s, 1H, –CH=N), 10.74 (s, 1H, –OH). MS (LCMS), $m/z$ = 611.2 $[M + H]^+$; calculated for $C_{39}H_{38}N_4O_3$ = 610.29.

**Preparation of chemodosimeter L.** To a stirred solution of compound **2** (0.25 mg, 0.41 mmol) in dry acetonitrile (10 ml), $K_2CO_3$ (1.5 equiv.) and a catalytic amount of KI were added. After 30 min, 2,4-dinitrofluorobenzene (0.076 mg, 0.41 mmol) was added dropwise to the stirred suspension, and the resulting mixture was then refluxed for 8 h. After the completion of the reaction (monitored by TLC), solvent was evaporated under vacuum and the residue was extracted with dichloromethane/water. The organic layer was dried over anhydrous sodium sulfate and then evaporated under vacuum. Then, the residue was chromatographed on silica gel (60–120 mesh) to give pure compound **L** as a yellow solid in 85% yield; m.p. > 250 °C. $^1$H-NMR ($CDCl_3$, 500 MHz) $\delta$ (ppm): 1.16 (t, 12H, $J$ = 8.5 Hz, $-NCH_2CH_3$), 3.33 (t, 8H, $J$ = 8.5 Hz, $-NCH_2CH_3$), 6.30 (d, 2H, $J$ = 9 Hz), 6.49 (s, 2H), 6.61 (d, 2H, $J$ = 10.5 Hz), 6.82 (t, 1H, $J$ = 11.5 Hz), 7.13–7.19 (m, 3H), 7.47–7.55 (m, 3H), 7.89 (s, 2H), 8.06 (t, 2H, $J$ = 8.5 Hz), 8.19 (dd, 1H, $J$ = 2.5 Hz & 11.5 Hz), 8.87 (d, 1H, $J$ = 3 Hz), 9.33 (s, 1H, –CH=N). $^{13}$C NMR ($CDCl_3$, 75 MHz) $\delta$ (ppm): 12.48, 44.58, 67.91, 98.02, 108.32, 116.84, 121.78, 122.78, 122.84, 124.01, 124.89, 127.22, 128.31, 128.66, 128.94, 129.30, 129.75, 130.07, 131.02, 131.35, 134.12, 138.32, 148.89, 148.98, 149.10, 149.51, 154.51, 166.10. MS (HRMS): ($m/z$, %): 777.3034 [(M + H$^+$), 100%]; calculated for $C_{45}H_{40}N_6O_7$ = 776.2958.

## Conflicts of interest

There are no conflicts to declare.

## Acknowledgements

SM would like to give special thanks to UGC, New Delhi, India for the DSK Postdoctoral fellowship (award no. F.4-2/2006(BSR)/CH/17-18/0097). SKM and SP thank Haldia Government College for partial laboratory facility. DM is very much grateful to the DST, Government of India, for providing the INSPIRE Faculty Fellowship (DST/INSPIRE/04/2016/001948).

## Notes and references

1 (*a*) *Gold: Progress in Chemistry, Biochemistry and Technology*, ed. H. Schmidbaur, Wiley, Chichester, 1999; (*b*) *Gold Chemistry Applications and Future Directions in the Life Sciences*, ed. F. Mohr, Wiley-VCH, Weinheim, 2009; (*c*) S. Singha, D. Kim, H. Seo, S. W. Cho and K. H. Ahn, *Chem. Soc. Rev.*, 2015, **44**, 4367–4399; (*d*) J. F. Zhang, Y. Zhou, J. Yoon and J. S. Kim, *Chem. Soc. Rev.*, 2011, **40**, 3416–3429.
2 (*a*) A. S. K. Hashmi and M. Rudolph, *Chem. Soc. Rev.*, 2008, **37**, 1766–1775; (*b*) G. J. Hutchings, M. Brust and H. Schmidbaur, *Chem. Soc. Rev.*, 2008, **37**, 1759–1765; (*c*) I. Braun, A. M. Asiri and A. S. K. Hashmi, *ACS Catal.*, 2013, **3**, 1902–1907.
3 (*a*) *Modern Supramolecular Gold Chemistry: Gold-Metal Interactions and Applications*, ed. A. Laguna, Wiley-VCH, Weinheim, 2008; (*b*) X. Ren and M. An, *RSC Adv.*, 2018, **8**, 2667–2677; (*c*) R. Sardar, A. M. Funston, P. Mulvaney and R. W. Murray, *Langmuir*, 2009, **25**, 13840–13851.
4 (*a*) L. E. V. Vlerken and M. M. Amiji, *Expert Opin. Drug Delivery*, 2006, **3**, 205–216; (*b*) M. M. O. Sulliva, J. J. Green and T. M. Przybycien, *Gene Ther.*, 2003, **10**, 1882–1890; (*c*) D. Pissuwan, S. M. Valenzuela and M. B. Cortie, *Trends Biotechnol.*, 2006, **24**, 62–67; (*d*) S. K. Balasubramanian, J. Jittiwat, J. Manikandan, C.-N. Ong, L. E. Yu and W. Y. Ong, *Biomaterials*, 2010, **31**, 2034–2042.
5 (*a*) R. Wilson, *Chem. Soc. Rev.*, 2008, **37**, 2028–2045; (*b*) X. Mao, Y. Ma, A. Zhang, L. Zhang and G. Liu, *Anal. Chem.*, 2009, **81**, 1660–1668; (*c*) S. Kumar and R. Richards-Kortum, *Nanomedicine*, 2006, **1**, 23–30; (*d*) N. Nitin, D. J. Javier and R. Richards-Kortum, *Bioconjugate Chem.*, 2007, **18**, 2090–2096.
6 (*a*) C. D. Pina, E. Falletta, L. Prati and M. Rossi, *Chem. Soc. Rev.*, 2008, **37**, 2077–2095; (*b*) D. J. Gorin and F. D. Toste, *Nature*, 2007, **446**, 395–403; (*c*) Y. Liu, F. Song and S. Guo, *J. Am. Chem. Soc.*, 2006, **128**, 11332–11333; (*d*) Z. Li, C. Brouwer and C. He, *Chem. Rev.*, 2008, **108**, 3239–3265.
7 (*a*) N. Duman, S. E. Evans, Ö. Karadağ, S. Aşçıoğlu, B. Şener, S. Kiraz and S. Şahin, *Int. J. Dermatol.*, 2014, **53**, 1286–1292; (*b*) I. Ott, *Coord. Chem. Rev.*, 2009, **253**, 1670–1681; (*c*) M. Navarro, *Coord. Chem. Rev.*, 2009, **253**, 1619–1626.
8 (*a*) L. Messori and G. Marcon, Gold Complexes in the Treatment of Rheumatoid Arthritis, *Metal Ions and their Complexes in Medication*, CRC Press, 2004; (*b*) C. F. Shaw, *Chem. Rev.*, 1999, **99**, 2589–2600; (*c*) A. Locke and E. R. Main, *J. Am. Med. Assoc.*, 1928, **90**, 259–260.
9 C. J. Fleming, E. L. Salisbury, P. Kirwan, D. M. Painter and R. S. Barnetson, *J. Am. Acad. Dermatol.*, 1996, **34**, 349–351.
10 (*a*) M.-T. Lee, T. Ahmed and M. E. Friedman, *J. Enzyme Inhib. Med. Chem.*, 1989, **3**, 23–33; (*b*) A. Habib and M. Tabata, *J. Inorg. Biochem.*, 2004, **98**, 1696–1702; (*c*) C. M. Goodman, C. D. McCusker, T. Yilmaz and V. M. Rotello, *Bioconjugate Chem.*, 2004, **15**, 897–900.
11 (*a*) E. Nyarko, T. Hara, D. J. Grab, A. Habib, Y. Kim, O. Nikolskaia, T. Fukuma and M. Tabata, *Chem. – Biol. Interact.*, 2004, **148**, 19–25; (*b*) J. R. E. Jones, *J. Exp. Biol.*, 1940, **17**, 408–415.
12 (*a*) J. A. Whitehead, G. A. Lawrance and A. McCluskey, *Aust. J. Chem.*, 2004, **57**, 151–155; (*b*) T. T. Chao, *Econ. Geol.*, 1969, **64**, 287–290; (*c*) *Methods Manual Vol. 1: Gold Analysis in Alkaline Cyanide Solutions*, ed. T. J. Gilbert, A Society of Mineral Analysts Publication, 1989; (*d*) A. Scheffer, C. Engelhard, M. Sperling and W. Buscher, *Anal. Bioanal. Chem.*, 2008, **390**, 249–252.
13 (*a*) G. M. Schmid and G. W. Bolger, *Clin. Chem.*, 1973, **19**, 1002–1005; (*b*) G. S. Reddi and C. R. M. Rao, *Analyst*, 1999, **124**, 1531–1540; (*c*) P. Braun in *Methods Manual, Vol. 1: Gold Analysis in Alkaline Cyanide Solutions*, ed. T. J. Gilbert, Society of Mineral Analysts, Sparks, 1989, pp. 6–20.
14 (*a*) T. L. Mako, J. M. Racicot and M. Levine, *Chem. Rev.*, 2019, **119**, 322–477; (*b*) D. Wu, A. C. Sedgwick, T. Gunnlaugsson, E. U. Akkaya, J. Yoon and T. D. James, *Chem. Soc. Rev.*, 2017, **46**, 7105–7123.
15 (*a*) J. Y. Choi, G.-H. Kim, Z. Guo, H. Y. Lee, K. M. K. Swamy, J. Pai, S. Shin, I. Shin and J. Yoon, *Biosens. Bioelectron.*, 2013, **49**, 438–441; (*b*) M. Dong, Y.-W. Wang and Y. Peng, *Org. Lett.*, 2010, **12**, 5310–5313.
16 (*a*) E. Karakus, M. Åinci and M. Emrullahoğlu, *Chem. Commun.*, 2014, **50**, 1119–1121; (*b*) J.-B. Wang, Q.-Q. Wu, Y.-Z. Min, Y.-Z. Liu and Q.-H. Song, *Chem. Commun.*, 2012, **48**, 744–746.
17 (*a*) H. Seo, M. E. Jun, O. A. Egorova, K. H. Lee, K. T. Kim and K. H. Ahn, *Org. Lett.*, 2012, **14**, 5062–5065; (*b*) N. Y. Patil, V. S. Shinde, M. S. Thakare, P. H. Kumar, P. R. Bangal, A. K. Barui and C. R. Patra, *Chem. Commun.*, 2012, **48**, 11229–11231.
18 (*a*) E. Karakuş, G. Çakan-Akdoğan and M. Emrullahoğlu, *Anal. Methods*, 2015, **7**, 8004–8008; (*b*) S. Adhikari, S. Mandal, A. Ghosh, P. Das and D. Das, *J. Org. Chem.*, 2015, **80**, 8530–8538.
19 (*a*) H. Seo, M. E. Jun, O. A. Egorova, K. H. Lee, K. T. Kim and K. H. Ahn, *Org. Lett.*, 2012, **14**, 5062–5065; (*b*) S. Kambam, B. Wang, F. Wang, Y. Wang, H. Chen, J. Yin and X. Chen, *Sens. Actuators, B*, 2015, **209**, 1005–1010.
20 (*a*) H. Seo, M. E. Jun, K. Ranganathan, K.-H. Lee, K.-T. Kim, W. Lim, Y. M. Rhee and K. H. Ahn, *Org. Lett.*, 2014, **16**, 1374–1377; (*b*) N. T. Patil, V. S. Shinde, M. S. Thakare, P. H. Kumar, P. R. Bangal, A. K. Barui and C. R. Patra, *Chem. Commun.*, 2012, **48**, 11229–11231; (*c*) Y. Yang, B. Bai, M. Jin, Z. Xu, J. Zhang, W. Li, W. Xu, X. Wang and C. Yin, *Biosens. Bioelectron.*, 2016, **86**, 939–943; (*d*) X. Cao, W. Lin and Y. Ding, *Chem. – Eur. J.*, 2011, **17**, 9066–9069.
21 (*a*) L. Yuan, W. Lin, Y. Yang and J. Song, *Chem. Commun.*, 2011, **47**, 4703–4705; (*b*) M. Ucnncu and M. Emrullahoglu, *Chem. Commun.*, 2014, **50**, 5884–5886.
22 (*a*) J. E. Park, M. G. Choi and S.-K. Chang, *Inorg. Chem.*, 2012, **51**, 2880–2884; (*b*) S. Y. Park, M. G. Choi, D. S. Lim and S.-K. Chang, *Dyes Pigm.*, 2019, **164**, 14–19.

 

23 (*a*) P. Chinapang, V. Ruangpornvisuti, M. Sukwattanasinitt and P. Rashatasakhon, *Dyes Pigm.*, 2015, **112**, 236–238; (*b*) J. Wang, W. Lin, L. Yuan, J. Song and W. Gao, *Chem. Commun.*, 2011, **47**, 12506–12508.

24 (*a*) C. Canturk, M. Ucuncu and M. Emrullahoğlu, *RSC Adv.*, 2015, **5**, 30522–30525; (*b*) W. Wang, Y. Huang, S. Wang, Y. Zhou, W. Huang, Y. Feng, W. Zhang, W. Yu, Q. Zhou, M. Chen and M. Fang, *Spectrochim. Acta, Part A*, 2017, **187**, 110–118.

25 M. Beija, C. A. M. Afonso and J. M. G. Martinho, *Chem. Soc. Rev.*, 2009, **38**, 2410–2433.

26 M. She, Z. Yang, L. Hao, Z. Wang, M. Obst Luo, P. Liu, Y. Shen, S. Zhang and J. Li, *Sci. Rep.*, 2016, **6**, 28972.

27 (*a*) M. Emrullaholu, M. Üçüncü and E. Karakus, *New J. Chem.*, 2015, **39**, 8337–8341; (*b*) B. Wang, T. Fu, S. Yang, J. Li and Y. Chen, *Anal. Methods*, 2013, **5**, 3639–3641.

28 S. Mondal, S. K. Manna, S. Pathak, A. A. Masum and S. Mukhopadhyay, *New J. Chem.*, 2019, **43**, 3513–3519.

29 Y. Liang, R. Wang, G. Liu and S. Pu, *ACS Omega*, 2019, **4**, 6597–6606.

30 (*a*) A. D. Becke, *J. Chem. Phys.*, 1993, **98**, 5648–5662; (*b*) C. Lee, W. Yang and R. G. Parr, *Phys. Rev. B: Condens. Matter Mater. Phys.*, 1988, **37**, 785–799; (*c*) B. Miehlich, A. Savin, H. Stoll and H. Preuss, *Chem. Phys. Lett.*, 1989, **157**, 200–206; (*d*) J. D. Dill and J. A. Pople, *J. Chem. Phys.*, 1975, **62**, 2921–2923.

31 M. J. Frisch, G. W. Trucks, H. B. Schlegel, G. E. Scuseria, M. A. Robb, J. R. Cheeseman, G. Scalmani, V. Barone, G. A. Petersson, H. Nakatsuji, X. Li, M. Caricato, A. V. Marenich, J. Bloino, B. G. Janesko, R. Gomperts, B. Mennucci, H. P. Hratchian, J. V. Ortiz, A. F. Izmaylov, J. L. Sonnenberg, D. Williams-Young, F. Ding, F. Lipparini, F. Egidi, J. Goings, B. Peng, A. Petrone, T. Henderson, D. Ranasinghe, V. G. Zakrzewski, J. Gao, N. Rega, G. Zheng, W. Liang, M. Hada, M. Ehara, K. Toyota, R. Fukuda, J. Hasegawa, M. Ishida, T. Nakajima,Y. Honda, O. Kitao, H. Nakai, T. Vreven, K. Throssell, J. A. Montgomery, Jr, J. E. Peralta, F. Ogliaro, M. J. Bearpark, J. J. Heyd, E. N. Brothers,K. N. Kudin, V. N. Staroverov, T. A. Keith, R. Kobayashi, J. Normand, K. Raghavachari, A. P. Rendell, J. C. Burant, S. S. Iyengar, J. Tomasi, M. Cossi, J. M. Millam, M. Klene, C. Adamo, R. Cammi, J. W. Ochterski, R. L. Martin, K. Morokuma, O. Farkas, J. B. Foresman and D. J. Fox, *Gaussian 16, Revision C.01*, Gaussian, Inc., Wallingford CT, 2016.